Desalination and Water Treatment
www.deswater.com

doi:10.5004/dwt.2019.24586

166 (2019) 24–34
October

Efficient removal of copper and lead from aqueous solution by magnetic biochar: Magnetization, adsorption, separation, and desorption

Zhifang Zhou[a,b], Baiping Zhao[c], Youxian Zhang[b,*], Hanxue Sun[a], Jixiang Chen[a], Tao Huang[b]

[a]*College of Petrochemical Technology, Lanzhou University of Technology, Lanzhou 730050, China*
[b]*Key Laboratory for Environmental Pollution Prediction and Control, College of Earth and Environmental Sciences, Lanzhou University, Lanzhou 730000, China, email: zhangyx0931@163.com (Y. Zhang)*
[c]*Lanzhou Construction Engineering Exploration and Design co. LTD, Lanzhou 730000, China*

Received 15 January 2019; Accepted 16 June 2019

ABSTRACT

Efficient removal of heavy-metal ions from water is of great importance for addressing the issue of environmental pollution. In this work, a novel magnetic biochar was fabricated by loading Fe_3O_4 on straw-oriented biochar (Fe_3O_4@BIO) through co-precipitation method. The preparation conditions were optimized, and the best Fe_3O_4@BIO synthesis was at BIO/Fe_3O_4 weight ratio of 5:1 to 3:1. The synthesis led to higher surface area and higher adsorption capacity for Cu^{2+} (143.2 mg/g) but relatively low capacity for Pb^{2+} (463.8 mg/g) as compared with non-magnetic biochar (56.1 and 665.4 mg/g, respectively). This means that different mechanisms dominated the adsorption processes for Cu^{2+} and Pb^{2+}. After four times of regeneration and reuse, the adsorption capacity retained 60%–70% of the level in the initial situation. Overall, our magnetic biochars are considered suitable for use in wastewater treatment processes because of their excellent heavy-metal adsorption ability and easy recovery after use.

Keywords: Magnetic biochar; Adsorption; Copper(II); Lead(II)

1. Introduction

Heavy-metal ions Cu^{2+} and Pb^{2+} are common pollutants in chemical, metallurgy, mining, electroplate, coking, and other related industries. When they are present or discharged at certain concentrations, they can be injurious and toxic to aquatic ecosystems since they resist decomposition and because they can accumulate in organisms; hence, their presence in water is a critical general health issue. Exposure to copper ions can cause lethargy, DNA damage, gastrointestinal bleeding, and hypertension [1], while lead exposure can result in anemia, chills, dysfunction, and diarrhea of kidney [2]. Their concentration in industrial wastewater can reach thousands of milligrams per liter. Thus, the separation and recycling of these pollutants has progressed into a critical issue.

Several methods have already been developed recently to remove heavy metals from solutions, such as chemical precipitation, ion exchange, filtration, electroplating, reverse osmosis, and adsorption [3]. Among these technologies, adsorption is considered as a reliable modern technology. It is preferred by industries because of its easy operation, high efficiency, and low cost of production. A series of materials such as activated carbon, fly ash, zeolites, and montmorillonite have been reported to have excellent properties for the removal of heavy metals from solutions [4–6]. It is ceratin that the powdered form of adsorbents are more efficient at pollutant removal than the granular form. Activated carbon is considered as the best adsorbent because it provides large surface area and hence high adsorption capacity [7]. But in recent studies, biochar that is similar to activated carbon and produced via thermal decomposition of biomass rich in carbon constituents, both of which belong to black carbon, has been shown to have better characteristics than activated carbon for metal removal [8].

Due to the presence of the rich porous structure and various functional groups, biochar exhibited a great poten-

*Corresponding author.

tial for heavy meals adsorption in wastewater. Commonly the feedstock materials for biochar in studies are agricultural wastes including sawdust, peanut shells, bagasse, rice straw, fruit peel and so on [8]. As the research into biochar has been great active in recent years, various kind of raw materials have been applied and studied to remove heavy metals such as daily manure, marine macro-algae and wastewater sludge [9–11]. But the output of these raw materials' are lower than agricultural wastes, and manufactured biochars' adsorption characteristic are also not as well as those biochar derived from agricultural wastes [8]. Moreover, many investigations of biochar and magnetic biochars have been biased toward the study of organic materials and anionic heavy metals in order to emphasize the adsorption ability of biochars, whereas studies related to cationic heavy metals adsorption are lacking [10]. It is necessary to found the biochar with abundant raw materials source and excellent adsorption capacity for heavy metals.

In addition, powdered biochar adsorbents can be difficult to separate from wastewater; therefore, they have been traditionally released with the process sludge into the environment, resulting in secondary pollution or another treatment process cost. Thus, magnetic separation is a suitable technology for the separation of adsorbents from wastewater. It is well known that Fe_3O_4 process rapidly magnetic responsibility when the external magnetic field is applied. Moreover, the adsorption properties of biochar such as adsorption capability, surface area, zeta potential, and kinetic and thermodynamic characteristics could be improved by loading magnetic materials [2,12,13], whereas some studies also find that the magnetization of the biochar by Fe_3O_4 partially reduce its adsorption efficiency due to the biochar's surface pores becoming plugged with iron oxide particles [2]. Generally, several previous studies have been conducted for the manufacture of magnetic biochar and the adsorption properties for heavy metals, but these studies mainly focus on the novelty of the material, the process of magnetization, and the separation efficiency of the adsorbents rather than the mechanism of the adsorption process, adsorption capacity and method optimization.

Thus, in order to provide an adsorbent with adequate raw materials and excellent sorption capability for heavy metals eliminating, a biochar derived from straw was selected for magnetic biochar (Fe_3O_4@BIO) synthesis by in situ co-precipitation in this paper. The sorption of Cu^{2+} and Pb^{2+} on biochar and Fe_3O_4@BIO composites were measured, and the adsorption capability of Fe_3O_4@BIO were optimized. The adsorption kinetics, thermodynamics, and the effect of some environmental factors are discussed. In addition, the adsorption mechanism was investigated by means of batch experiments, adsorption model, and characterization techniques.

2. Material and methods

2.1. Chemicals and material

All chemicals used in this study were analytically pure, including $FeSO_4{\cdot}7H_2O$, $FeCl_3{\cdot}6H_2O$, $Cu(NO_3)_2{\cdot}3H_2O$, $Pb(NO_3)_2$, NaCl, KCl, $MgCl_2$, $CaCl_2$, HNO_3, and NaOH. The stock solution of Cu^{2+} and Pb^{2+} (1000 mg/L) were prepared by dissolving $Cu(NO_3)_2{\cdot}3H_2O$, $Pb(NO_3)_2$ in distilled water (DW). A straw-oriented gasification biochar (BIO) was selected as the adsorbent. In brief, the agricultural straw purchased from the company of Yuzhongao (Henan, China) was air-dried in a fume cupboard, crushed by a pulverizer, pyrolyzed at approximately 550°C in a kiln for 2 h, and then ground until they pass through a 100-mesh sieve. The BIO was stored in a drying oven for subsequent study.

2.2. Fabrication of magnetic biochar

The preparation of magnetic biochar (Fe_3O_4@BIO) was similar to that in a previous study [10]. First, a certain mass of BIO was dispersed in 100 mL of DW and stirred by a magnetic stirrer. Second, 50 mL of $FeSO_4$ at a certain concentration was added to the above solution, and then 50 mL of $FeCl_3$ solution at a certain concentration was added. After thorough stirring for 15 min, 10 M NaOH solution was added dropwise to the BIO/Fe^{2+}/Fe^{3+} solution until the pH reached 10–11. The mixture was allowed to react for 8 h at room temperature, and the obtained Fe_3O_4@BIO was magnetically separated and washed with DW several times to remove the impurities. Finally, the solid sample was freeze-dried for 48 h. The concentration of $FeSO_4$ and $FeCl_3$ were calculated previously to synthesize different mass ration of Fe_3O_4 loaded onto BIO according to Eq. (1), the mass ration of BIO: Fe_3O_4 were ranging from 7:1 to 1:3. The adsorption capacity of these Fe_3O_4@BIO powders for Cu^{2+} and Pb^{2+} were measured, respectively.

$$Fe^{2+} + 2Fe^{3+} + 8OH^- \rightarrow Fe_3O_4 + 4H_2O \quad (1)$$

2.3. Characterization of the surface properties

The specific surface area was determined with the Brunauer–Emmett–Teller (BET) equation with multi point adsorption isotherms of N_2 at 77 K (Micro meritics ASAP 2020). The surface morphology was analyzed by scanning electron microscopy (SEM-EDS; S-4800/EX-350, Hitachi, Japan). The functional groups on the powder sample surface were recorded using Fourier transform infrared spectra (FTIR) over the spectral range of 4000–400 cm^{-1} at a resolution of 4 cm^{-1} by using pressed KBr discs. (Affinity-1, Shimadzu, Japan). The crystallographic structures were analyzed by power X-ray diffraction (XRD, X-Pert Pro MPD, Panalytical, Holland). The chemical compositions were confirmed by X-ray photo electron spectrometry (XPS, ESCSLAB 250Xi, Thermo Fisher, USA).

2.4. Batch sorption experiments

In batch experiments, a certain amount of BIO or Fe_3O_4@BIO was add to 50 mL polyethylene centrifuge tubes and mixed with a certain volume of Cu^{2+} or Pb^{2+} solution. The solid/liquid ratios of Cu^{2+} and Pb^{2+} solutions were fixed at 2:1 and 1:2, respectively. The adsorption isotherms were obtained by using the adsorption experimental results of the different Cu^{2+} and Pb^{2+} solutions with concentrations ranging from 100 to 1000 mg/L. The adsorption kinetics was examined at reaction time intervals ranging from 0.5 to 48 h with 500 mg/L heavy

metal solution at free pH. The effect of pH on adsorption capacity was studied by adjusting pH values from 2 to 7 by using diluted HNO_3 and NaOH solution. The cations K^+, Ca^{2+}, Na^+, and Mg^{2+} at concentrations of 0–50 mmol/L were used to study the effect of competitive adsorption. Except of adsorption kinetics other adsorption tests were conducted 48 h. After a predetermined time of shaking at 180 rpm in a shaker, the supernatant was filtered through a 0.45 μm membrane, treated with 1 mol/L of nitric acid, and stored at 4°C until analysis. The residual concentration of metals remaining in adsorption solution was analyzed by an atomic absorption spectrophotometer (ICE3500, Thermo Fisher, USA) or by inductively coupled plasma mass spectrometry.

The adsorption capacity (Q_e, mg/g) of BIO or Fe_3O_4@BIO for heavy-metal ions was calculated by the following equation:

$$Q_e = \frac{(C_0 - C_e) \times V}{m} \quad (2)$$

where C_0 and C_e (mg/L) are, respectively, the initial and equilibrium concentrations of the heavy-metal ions. V (L) is the volume of the adsorption solution, and m (g) is the mass of adsorbent.

3. Results and discussion

3.1. Characterization of BIO before and after magnetization

3.1.1. Optimum Fe_3O_4 loading for magnetization

Fig. 1a shows the adsorption capacity and recovery efficiency of BIO and Fe_3O_4@BIO for Cu^{2+}. It is observed that with increasing BIO/Fe_3O_4 mass ratio, the adsorption of Cu^{2+} on Fe_3O_4@BIO increased up to 170.3 mg/g at a mass ratio of 5:1 and then decreased with further increase of the BIO/Fe_3O_4 mass ratio. As for Pb^{2+} (Fig. 1b), the highest adsorption capacity (674 mg/g) was observed as the BIO/Fe_3O_4 weight ratio was fixed at 1:0; it was always decreasing as when the loading had more Fe_3O_4. In addition, the high proportion of Fe_3O_4 led to high recovery efficiency and large BET surface area, and the recovery efficiency reached 87.5% at a mass ratio of 5:1. Comparison with BIO showed that the BET surface area of Fe_3O_4@BIO reached 124.3 m^2/g at the lowest BIO/Fe_3O_4 ratio in this study. The synthetic Fe_3O_4 through co-precipitation was almost nanoscale; it could cover the surface of BIO and could react with functional groups such as C=O, C–O, C–H, and O–H, as can be concluded from FTIR analysis (Fig. 3). This resulted in a change in Fe_3O_4@BIO adsorption capability for metal ions. So, it is essential to determine the optimum BIO/Fe_3O_4 mass ratio that maximizes the separation efficiency of Fe_3O_4@BIO and the adsorption of copper without sacrificing much of its adsorption capacity for lead.

In order to achieve the high adsorption capacity and recovery efficiency, the optimum BIO/Fe_3O_4 mass ratio was fixed at 5:1 to 3:1 (Fig. 1). In the subsequent study, the adsorbent was synthesized at a ratio of 3:1 because the Fe_3O_4@BIO composite can maintain the magnetic properties and adsorption capability during multiple reuses.

3.1.2. Surface characterization

The surface morphology of BIO and Fe_3O_4@BIO were characterized by SEM-EDS. Fig. 2a shows that BIO exhibits a highly porous structure with a relatively smooth surface as compared with Fe_3O_4@BIO. The wrinkled surface and richer porous structure of the BIO allows the Fe_3O_4 to be more easily loaded onto or into the BIO. After magnetization, the Fe_3O_4 particles appeared on the surface of BIO, which exhibited a relatively rough surface as compared with the BIO. The appearance of the signal of Fe indicates that Fe_3O_4@BIO was successfully prepared (Fig. 2d).

The FTIR spectra of BIO, Fe_3O_4, and Fe_3O_4@BIO composite are presented in Fig. 3a. The peak at 3281–3644 cm^{-1} is assigned to the O–H stretching vibration, the peak at 1430 cm^{-1} is matched to the C=O stretching vibration, and the peaks within 1038 and 876 cm^{-1} are ascribed to the C–O stretching vibration and C–H plane deformation vibra-

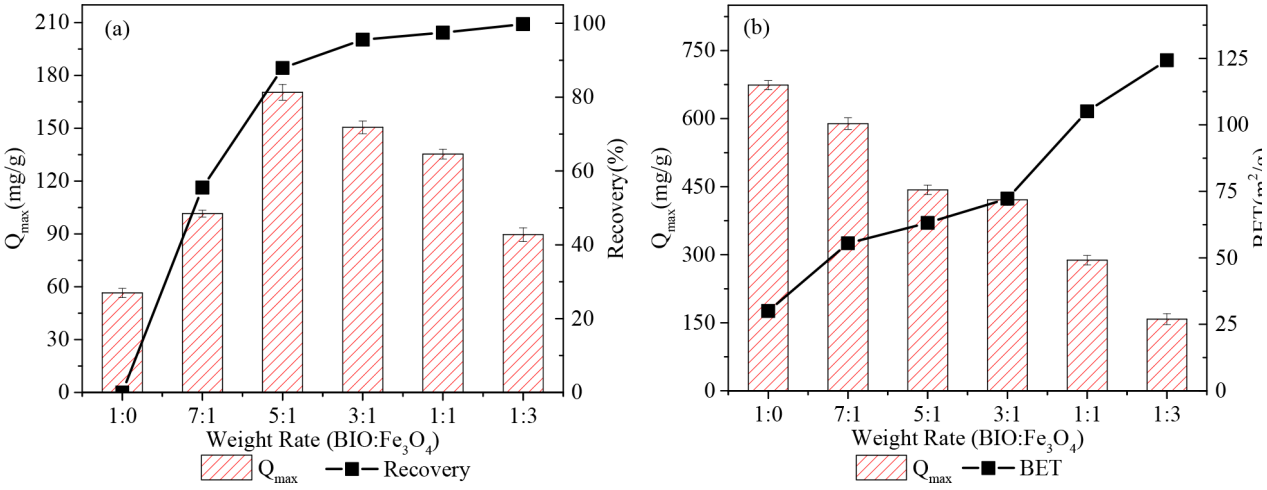

Fig. 1. The adsorption of BIO@Fe_3O_4 for Cu^{2+} (a) and Pb^{2+} (b) and the recovery efficiency (a) and BET (b) of BIO@Fe_3O_4 composite at different weight rate.

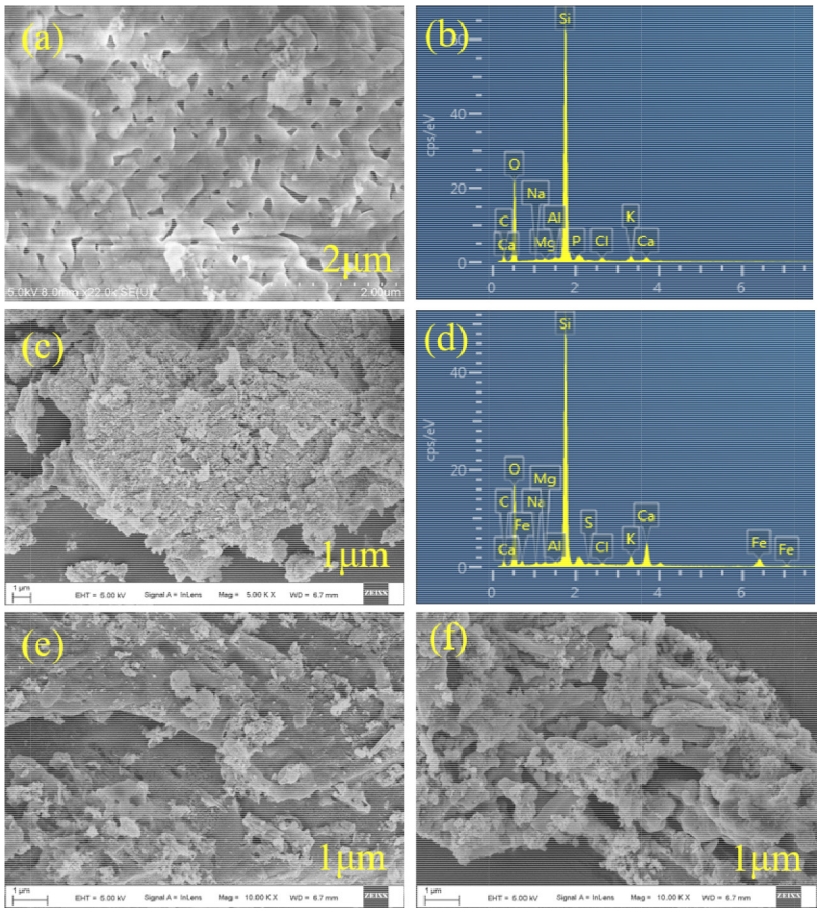

Fig. 2. The SEM-EDS of BIO (a and b) and BIO@Fe_3O_4 (c and d) before adsorption test, and the SEM of BIO@Fe_3O_4-Cu (e) and BIO@Fe_3O_4-Pb (f) after adsorption test.

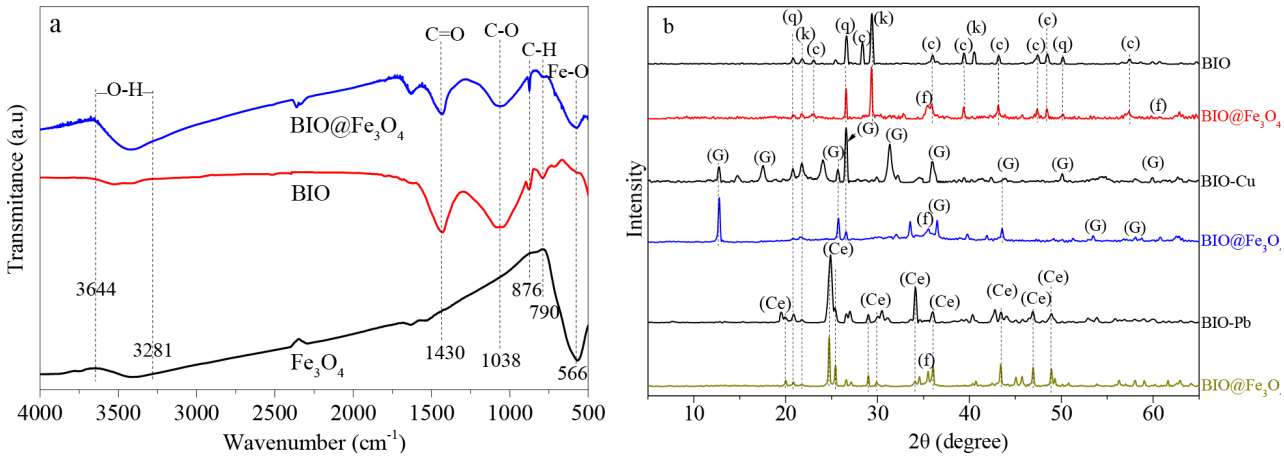

Fig. 3. The FTIR spectrums of Fe_3O_4, BIO and BIO@Fe_3O_4 (a) and XRD patterns of BIO and BIO@Fe_3O_4 before and after adsorption test (b). (q): SiO_2, (k): KCl, (c): $CaCO_3$, (f):Fe_3O_4, (Ce): $PbCO_3$, (G): Gerhardtite

tion, respectively [14,15]. The band at 566 cm^{-1} of Fe_3O_4 is attributed to the stretching vibration of Fe-O [10], which is also observed in the Fe_3O_4@BIO composite and similar with other related study [16]. Comparison with BIO revealed that the bonds of Fe_3O_4@BIO appeared at the same wavenumber; this shows that the basic surface characteristics of the BIO remains unchanged largely after magnetization by Fe_3O_4.

XRD patterns for BIO and Fe_3O_4@BIO are presented in Fig. 3b. The result indicates that the solid samples were dominated by calcite and quartz. For Fe_3O_4@BIO, it was observed new peaks at 2θ = 35.7°, 43.0°, 56.8°, 62.5°

(Fe_3O_4), and the shape of Fe_3O_4@BIO pattern did not change noticeably as compared with BIO. Similarly, XPS analysis showed that, the element Fe was successfully loaded onto the surface of BIO (Fig. 4). The Fe 2p peak further demonstrates that iron oxides in the composite are Fe_3O_4 rather than Fe_2O_3 [17], consistent with the result of XRD analysis.

3.2. Adsorption study

3.2.1. Adsorption kinetics

The effects of reaction time on adsorption capacity for Cu^{2+} and Pb^{2+} of BIO and Fe_3O_4@BIO are shown in Fig. 5. There was no obvious diffidence between BIO and Fe_3O_4@BIO for Pb^{2+} in terms of achieving adsorption equilibrium

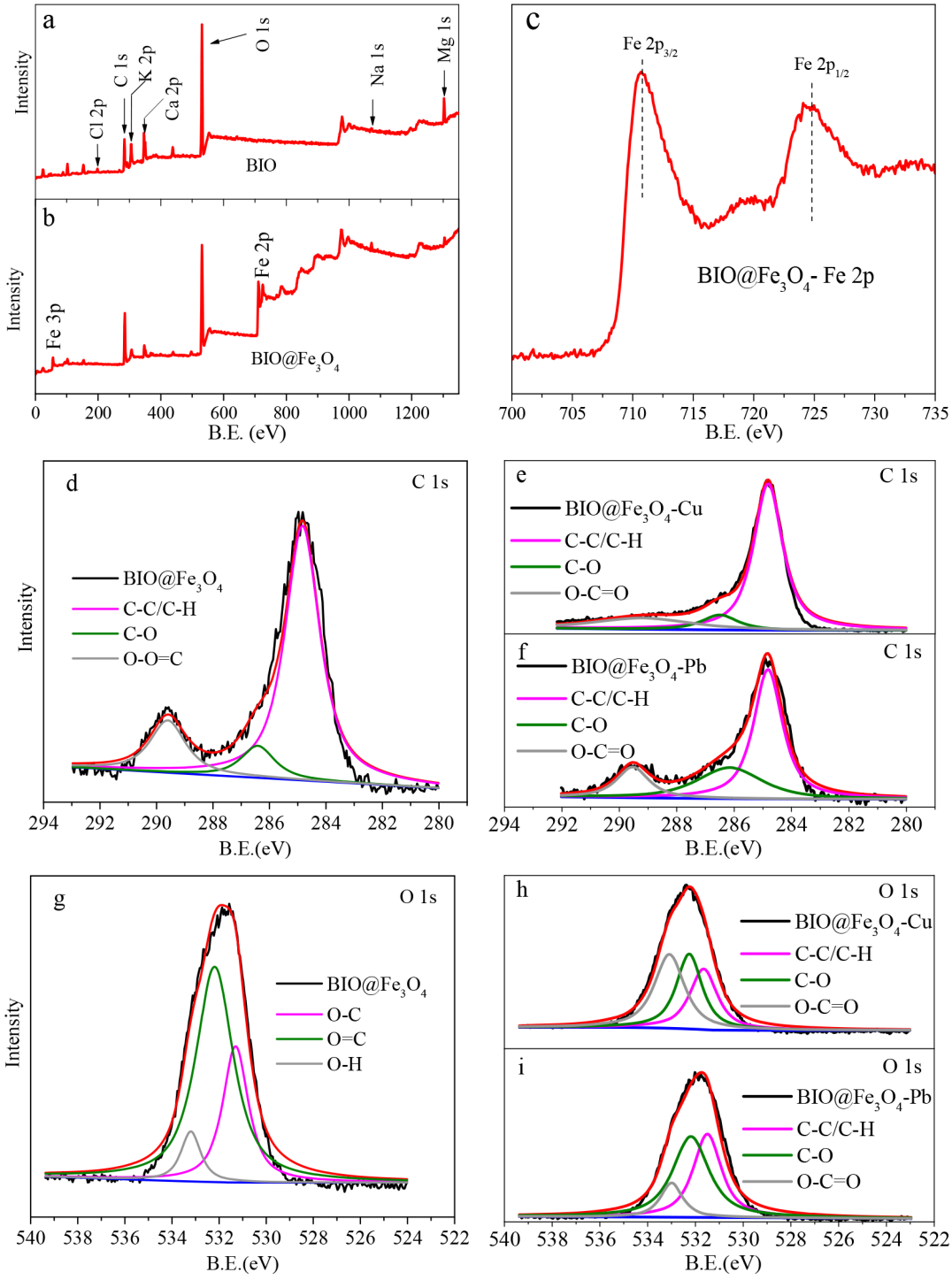

Fig. 4. The XPS of wide scan of BIO (a) and BIO@Fe_3O_4 (b), Fe 2p spectrum of BIO@Fe_3O_4 (c) composite, and C 1s and O 1s of BIO@Fe_3O_4 before (d and g) and after adsorption Cu (e and h) and Pb (f and i), respectively.

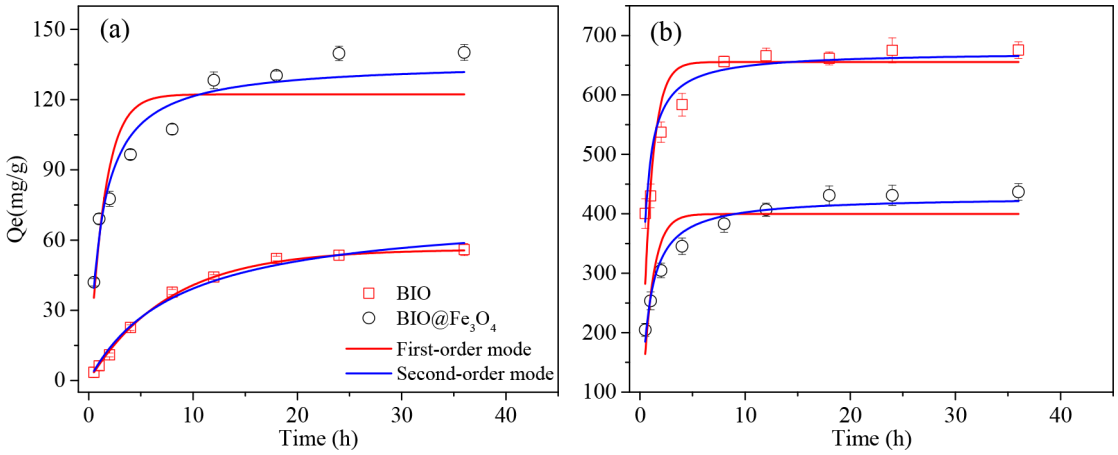

Fig. 5. Adsorption kinetics for Cu^{2+} (a) and Pb^{2+} (b) at 25°C.

(approximately 9 h), but for Cu^{2+} the Fe_3O_4 loading on BIO surface could shorten the equilibrium time from 18 to 12 h. It was observed that the adsorption capacity of Fe_3O_4@BIO for Cu^{2+} (122.2 mg/g) was almost two times higher than that of BIO (56.1 mg/g), whereas that for Pb^{2+} (435.6 mg/g) was lower than that of BIO (665.4 mg/g). In order to explore the mechanism of the adsorption process, the experimental data were analyzed by the pseudo-first-order [Eq. (1)] and the pseudo-second-order [Eq. (2)] models:

$$\log\left(q_e - q_t\right) = \log q_e - \frac{k_1}{2.303}\cdot \mathrm{t} \tag{3}$$

$$\frac{t}{q_t} = \frac{1}{k_2 q_e^2} + \frac{t}{q_e} \tag{4}$$

where q_t and q_e (mg/g) are adsorption capacity at time t and at equilibrium, respectively; k_1 and k_2 (h^{-1}) are the pseudo-first-order and pseudo-second-order adsorption rate constants, respectively. The fitted plots are shown in Fig. 5, and the parameters of these two models are summarized in Table 1. It can be easily concluded from these results that all of the correlation coefficients (R^2) of pseudo-second-order model are better than those of the pseudo-first-order model. In addition, the calculated value of q_e in the pseudo-second-order model was closer to the real value, indicating that electron transfer and the chemical adsorption are the rate-limiting step in the adsorption process [16].

3.2.2. Adsorption isotherms

The relationship between initial concentrations of the adsorbate and the adsorption capacity at a given temperature can be described by the adsorption isotherms (Fig. 6). This analysis can provide further information about the adsorption process and the optimum adsorption system for efficient separation of heavy metals from solution. Two isotherm models were used to fit the isotherm data: Langmuir [Eq. (3)] and Freundlich [Eq. (4)]. The Langmuir isotherm assumes that the adsorption occurs at a mono layer, with no interaction between the adsorbed molecule [18,19]. The Freundlich isotherm assumes multilayer and non-ideal adsorption on a heterogeneous surface with a non-uniform distribution of adsorption activation energy [19]. These non-linear equations can be described as follows:

$$Q_e = \frac{K_L Q_{max} C_e}{1 + K_L C_e} \tag{5}$$

$$Q_e = K_F C_e^m \tag{6}$$

where K_L (L/mg) is the Langmuir equilibrium adsorption constant related to the affinity of binding sites, and K_F ($mg^{(1-n)}L^n/g$) is the Freundlich affinity coefficient, respectively. Q_{max} (mg/g) is the maximum adsorption capacity of the sorbent, C_e (mg/L) is the equilibrium concentration of the sorbate, m is the Freundlich linearity constant, and Q_e is the adsorption capacity at equilibrium (mg/g). The Langmuir and Freundlich parameters are listed in Table

Table 1
Best-fit model parameters for the adsorption kinetics

Metal	Adsorbent	First-order			Second-order		
		Q_{max}, mg/g	k_1	R^2	Q_{max} mg/g	k_2	R^2
Cu	BIO	56.1	0.13	0.99	60.5	0.0016	0.99
	BIO@ Fe_3O_4	122.2	0.68	0.89	136.2	0.006	0.96
Pb	BIO	665.4	1.12	0.80	672.3	0.004	0.85
	BIO@ Fe_3O_4	435.6	1.06	0.82	428.9	0.0035	0.96

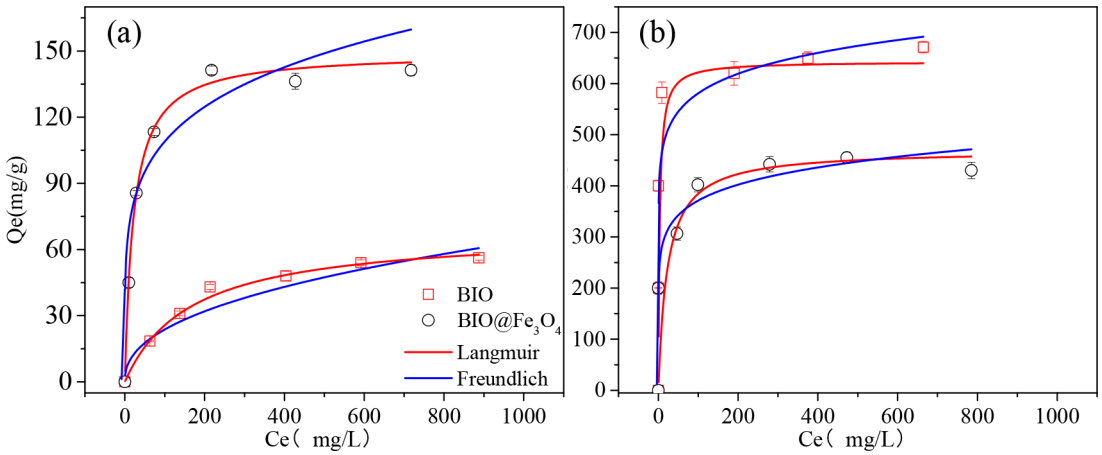

Fig. 6. Adsorption isotherms for Cu^{2+} (a) and Pb^{2+} (b) at 25 °C.

Table 2
Best-fit model parameters for the adsorption isotherms

Metal	Adsorbent	Langmuir			Freundlich		
		Q_{max}, mg/g	K_L	R^2	K_f	m	R^2
Cu	BIO	66.4	0.006	0.99	3.2836	0.4294	0.93
	BIO@ Fe_3O_4	149.2	0.046	0.99	44.5745	0.1941	0.78
Pb	BIO	642.9	0.293	0.95	380.34	0.0919	0.93
	BIO@ Fe_3O_4	470.2	0.045	0.90	217.63.	0.1159	0.76

2. Q_{max} of Fe_3O_4@BIO for Cu^{2+} was 149.2 mg/g, which was approximately 2.2 times higher than that of BIO; Q_{max} of BIO@Fe_3O_4 for Pb^{2+} decreased by 26.9% relative to that of BIO. The reason for this opposite result may be attributed to different adsorption mechanisms for Cu^{2+} and Pb^{2+}. The bound of Pb^{2+} may dominated by both the physisorption and chemisorption processes such as surface co-precipitation and ion exchange. But for Cu^{2+}, the adsorption process may be controlled by the physical absorption or electrostatic interaction and shared with chemisorption. In addition, all R^2 values of the Langmuir are higher than Freundlich, as shown in Table 2, suggesting that the sorption of Cu^{2+} and Pb^{2+} on both BIO and Fe_3O_4@BIO is dominated by mono layer adsorption [16].

3.2.3. Effect of initial pH

It is well known that pH plays an important role in the adsorption process because it affects the degree of ionization and speciation of the heavy metals, as well as the charges and states of the functional groups of the adsorbent. As the magnetic particles consist of iron oxides, a heavily acidic condition can induce the leaching of iron ions into the wastewater, thus possibly having a negative effect on magnetic separation. Fig. 7 shows the effect of the initial pH on the sorption capability and recovery efficiency of Fe_3O_4@BIO. With increasing pH value from 2 to 7, the adsorbent capability of Fe_3O_4@BIO increased from 48.4 to 226.1 mg/g for Cu^{2+} and from 150.6 to 616.1 mg/g for Pb^{2+}. In addition, the recovery efficiency of Fe_3O_4@BIO composite was enhanced with the increase in the pH value. At the lowest pH, the adsorbent recovery efficiencies of the two adsorption systems were below 50%; when the pH rose to ≥5, almost 90% of the Fe_3O_4@BIO could be recovered.

Usually at relatively low pH, copper ions and lead ions commonly exist as bivalent ions, and H^+ at high concentration can compete with them for adsorption sites. A high H^+ activity promotes protonation of the surface groups on the adsorbent and thus repulsion of the heavy-metal ions [19], resulting in a decline of adsorption capability. Along with increase in pH, the decrease in H^+ activity could reduce the competitive adsorption, resulting in an increase in adsorption capacity [19]. When the pH was close to 7 under the study conditions, the heavy metals could react with OH^- to form precipitations promoting the removal of Cu^{2+} and Pb^{2+} from solutions.

3.2.4. Effect of coexisting ions

In addition to pH, coexisting of ions such as Na^+, K^+, Ca^{2+}, and Mg^{2+}, which are abundant in the natural environment, can also compete with heavy metals for adsorption sites and thus have an effect on adsorbent capability. In Fig. 8, the adsorption capacity of Fe_3O_4@BIO for Cu^{2+} and Pb^{2+} in the presence of other cations is lower than that of blank. When these four cations were added, the adsorption capacity was markedly inhibited in the following order: $Ca^{2+} > Mg^{2+} > K^+ > Na^+$. The adsorption capacity decreased with increasing concentration of

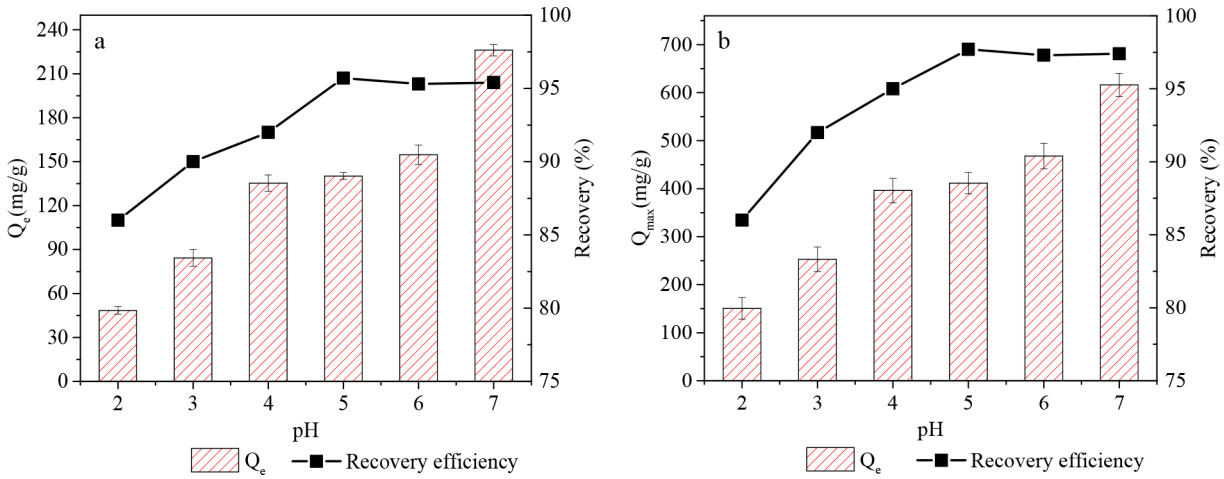

Fig. 7. The effect of pH on Fe_3O_4@BIO sorption capacity (Q_e) and its recovery efficiency for Cu^{2+} (a) and Pb^{2+} (b).

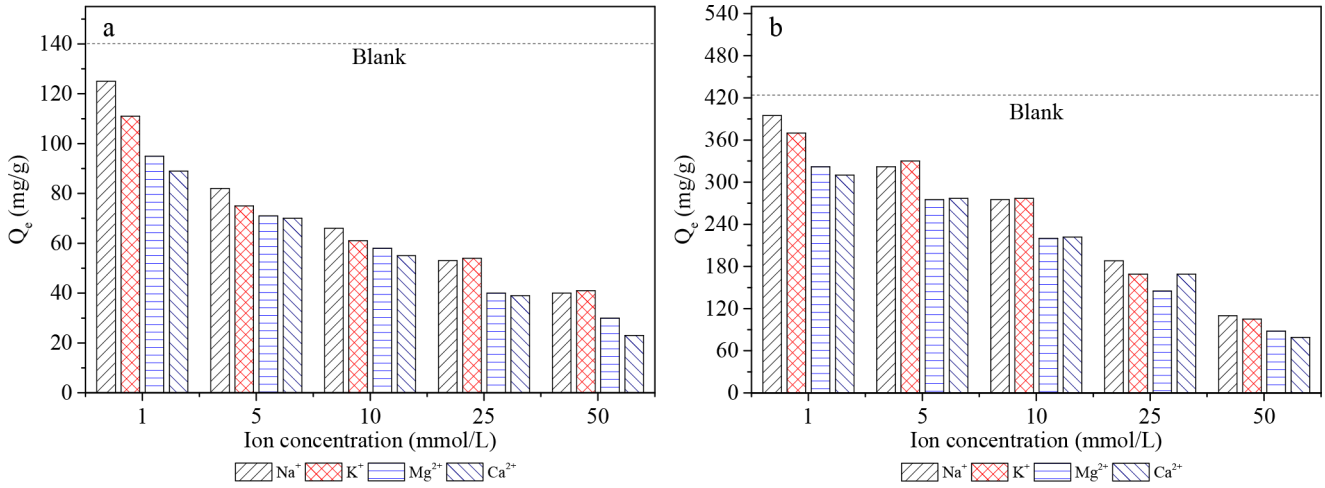

Fig. 8. The effect of ion strength on Fe_3O_4@BIO sorption capacity for Cu^{2+} (a) and Pb^{2+} (b).

coexisting cation. Cation exchange and competition can explain these results, but the internal mechanism remains unclear [20]. In some studies, the ionic radii were considered as one of the reasons for competing adsorption [21,22]. The hydrated cation represents its effective form in the aqueous solution, and it has greater size than the ionic radius. As shown in Table 3 [23,24], the hydrated radii of related cations decrease in the following order: $Mg^{2+} > Ca^{2+} > Na^+ > K^+$, indicating that the adsorption capacity and the hydrated radii of the cations are in the reverse sequence under the same charge number conditions. However, another study pointed out that the adsorption capacity is affected by the ion hydration and the charge number of the ions. Therefore, the adsorption affinity of the coexisting cation ions could compared through the following equation, which is similar to Coulomb's electrostatic law:

$$F = k\frac{|q_1 q_2|}{r^2} \tag{7}$$

where k ($(N\cdot m^2)/C^2$) is a constant; q_1 (C) and q_2 are the charges of the adsorbent and ion, respectively; and r (m) is the distance between the charges. The higher was the F value of the coexisting ions, the stronger was the binding affinity and the more obvious was the inhibitory effect on the adsorption of Cu^{2+} and Pb^{2+} [16]. According to the calculation, the adsorption affinity decreases in the following order: $F_{Ca^{2+}} > F_{Mg^{2+}} > F_{K^+} > F_{Na^+}$, which is consistent with the experimental data in this study.

Table 3
The bare and hydrated radii of the cations

Ion	Ion radius (nm)	Hydrated radius (nm)
H_3O^+	0.115	0.28
Ca^{2+}	0.100	0.412
Mg^{2+}	0.072	0.428
Na^+	0.117	0.358
K^+	0.149	0.331
Cu^{2+}	0.073	0.325
Pb^{2+}	0.132	0.401

3.3. Adsorption mechanism

The adsorption process of heavy-metal ions can be generally concluded as physical and chemical binding mechanisms. The morphology of the surface of Fe_3O_4@BIO changed markedly after adsorption Cu^{2+} and Pb^{2+}, as shown in Figs. 2c, e, and f. Before adsorption, there are some pore structures and rough surface in Fe_3O_4@BIO, whereas, after adsorption experiment, the pore structure is blocked and disappeared completely, the surface of Fe_3O_4@BIO is becoming smooth, and the new compounds be generated with the shape of amorphous or crystalline granular, which suggest that surface co-precipitation had great contribution to the adsorption process. Through element analysis by XPS, the C 1s spectrum of Fe_3O_4@BIO was deconvoluted into three components (Fig. 4d): C–C/C–H at 284.83 eV, C–O at 286.40 eV, and O–O=C at 289.59 eV [16,19]. The O 1s spectrum was composed of three peaks for O–C, O=C, and O–H at binding energy (BEs) of 531.49, 532.18, and 532.99 eV, respectively [16,19]. The BEs of the C 1s and O 1s spectra of Fe_3O_4@BIO after adsorption Cu^{2+} and Pb^{2+} are compared in Table 4. Although the elements of Fe_3O_4@BIO after adsorption of Cu^{2+} and Pb^{2+} show the same functionalities as those of Fe_3O_4@BIO, there was a different for binding energy after adsorption. The change of the BEs values of Fe 2p was not significant, suggesting that the Fe atom does not participate in Cu^{2+} and Pb^{2+} chemical bonding adsorption. Whereas the BEs of C 1S and O 1s shifted, indicating that hydroxyl and carboxyl are the active position for adsorption Cu^{2+} and Pb^{2+} and involved in the adsorption process. According to the results of XRD analysis, the crystal structures of Fe_3O_4@BIO-Cu and Fe_3O_4@BIO-Pb mainly consisted of $Cu_2(OH)_3NO_3$ and $PbCO_3$, respectively. So the chemical process with new substances being produced is the one of the adsorption mechanisms.

Loading Fe_3O_4 conferred a larger BET surface area for BIO, making the Cu^{2+} adsorption capacity higher in a certain range while decreasing the Pb^{2+} adsorption capacity. However, as the weight ratio of Fe_3O_4 increased, the adsorption capacity of Fe_3O_4@BIO for Cu^{2+} was declined and that for Pb further decreased. This mainly resulted from the coating of Fe_3O_4 onto the BIO surface, which impeded the reaction between the surface of the adsorbent and heavy metals. Hence, it can be concluded that the adsorption mechanism for Cu^{2+} and Pb^{2+}on Fe_3O_4@BIO was controlled by physical process and sharing with chemical process, but their relative weight may be different for different metals resulting in the different of adsorption characteristic shown as Fig. 1.

3.4. Regeneration, reuse, and comparison

The recycle and reuse performance of Fe_3O_4@BIO was studied to decrease the usage cost. In this study, HNO_3 solution at pH 2.0 was used to conduct the regeneration. As shown in Fig. 9, both adsorption and recovery efficiency of Fe_3O_4@BIO gradually decreased with the increase in cycling times. After four times of regeneration (Fig. 9), the adsorption capacity of Fe_3O_4@BIO for both Cu^{2+} and Pb^{2+} remained at 45%–70% of its initial capacity and recovery efficiency. First, partly Fe_3O_4 was dissolved from the BIO surface in the process of regeneration. Second, H^+, which has small hydrated radius, can replace ions such as K^+, Ca^{2+}, Na^+, and Mg^{2+} at the same time, thus lowering the ion-exchange

Table 4
The binding energies of C, O, and Fe before and after adsorption

Sample	C 1s			O 1s			Fe $2p_{3/2}$
	C-C/C-H	C-O	O-O=C	O-C	O=C	O-H	
Fe_3O_4@BIO	284.83	286.40	289.59	531.49	532.18	532.99	712.45
Fe_3O_4@BIO-Cu	284.81	286.29	289.17	531.66	532.26	533.09	712.46
Fe_3O_4@BIO-Pb	284.81	286.15	289.22	531.30	532.20	533.20	712.45

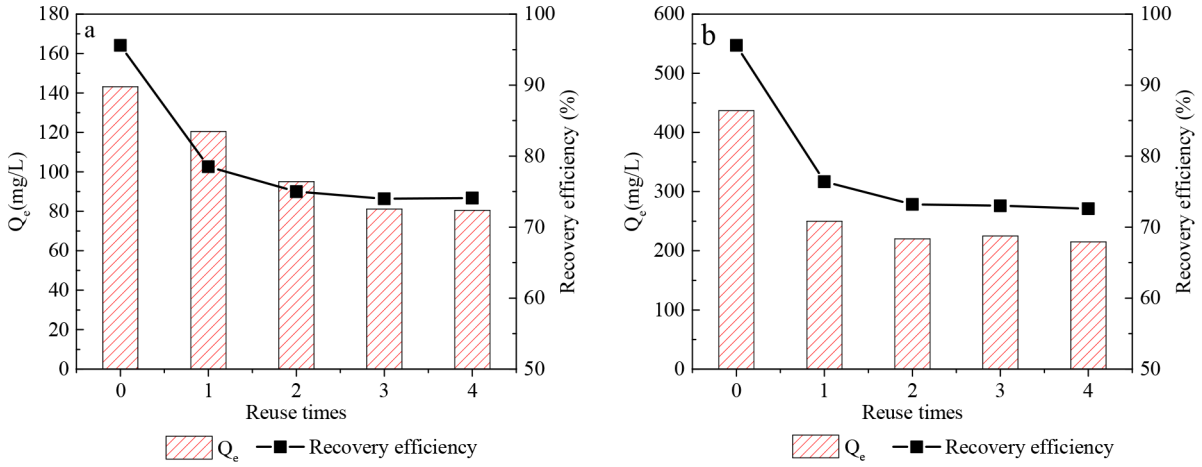

Fig. 9. The adsorption capacity (Q_e) and recovery efficiency of Fe_3O_4@BIO in regeneration cycle for Cu^{2+} (a) and Pb^{2+} (b).

capacity. Furthermore, some crystal structures of Fe_3O_4@BIO may be destroyed under acidic conditions, especially carbonate, which can be dissolved and cannot be regenerated. These reasons explain the decline of the adsorption capacity and recovery efficiency of the Fe_3O_4@BIO composite.

There is a comparison of maximum adsorption capacities between the Fe_3O_4@BIO and other reports, and the results are presented in Table 5. The adsorption capacity of Fe_3O_4@BIO for Cu^{2+} and Pb^{2+} is excellent, higher than that of other studies. Such comparison shows that Fe_3O_4@BIO synthesized by co-precipitation method is an efficient adsorbent for the treatment of wastewater with heavy-metal ions.

4. Conclusion

In this study, a magnetic adsorbent was synthesized, and its properties were investigated by SEM, FTIR spectroscopy, XPS, and XRD. Fe_3O_4@BIO had an adsorption capacity for Cu^{2+} higher than that of BIO in a certain range of BIO/Fe_3O_4 weight ratio but for Pb^{2+} that was lower. As the ratio continuously increased, both Cu^{2+} and Pb^{2+} adsorption capacity declined, while the BET surface area of the adsorbent and the separation behavior of the magnetic biochar increased. On the basis of these results, the optimum BIO/Fe_3O_4 weight ratio was found to be 5:1 to 3:1. We used 3:1 in this study, for which the adsorption capability for Cu^{2+} was 143.2 mg/g and that for Pb^{2+} was 463.8 mg/g. The adsorption mechanisms for Cu^{2+} and Pb^{2+} on Fe_3O_4@BIO were controlled by a physical process shared by a chemical process, but their relative weight may be different for different metals. Furthermore, the adsorption capacity could retain 60%–70% of the capacity after four times of regeneration and reuse. Overall, our magnetic biochar can be an alternative adsorbent for use in wastewater treatment processes because of their excellent heavy-metal adsorption ability and easy recovery after use. However, the regeneration process of the adsorbent method should be further studied to maintain good magnetic properties and heavy-metal adsorption capacity. This includes using different types and concentrations of regenerant and various regeneration processes.

Table 5
Comparison of adsorption capacities for Cu^{2+} and Pb^{2+} in various studies

Adsorbent	Modified method	Cu^{2+} (mg/g)	Pb^{2+} (mg/g)	References
Biochar	Magnetization	85.93	–	[25]
Biochar	–	11.34		[25]
Activated carbon	Phosphoric acid	19.6		[26]
Activated carbon	–	24.5		[26]
Biochar	–	56.1		This study
Biochar	Magnetization	143.2		This study
Biochar	Magnetization		52.4	[12]
Biochar	Magnetization		162.75	[13]
Activated carbon	–		99.5	[27]
Activated carbon	–		134.2	[28]
Biochar	–		665.4	This study
Biochar	Magnetization		463.8	This study

Acknowledgments

This work was financially supported by the Natural Science Foundation of China (30972275), the Youth Fund of the Natural Science Foundation, and the Youth Science (41503089) and Technology Foundation of Gansu Province, China (1606RJYA298).

References

[1] T. Aman, A.A. Kazi, M.U. Sabri, Q. Bano, Potato peels as solid waste for the removal of heavy metal copper (II) from waste water/industrial effluent, Colloids Surfaces B Biointerf., 63 (2008) 116–121.
[2] X. Zhou, Y. Liu, J. Zhou, J. Guo, J. Ren, F. Zhou, Efficient removal of lead from aqueous solution by urea-functionalized magnetic biochar: Preparation, characterization and mechanism study, J. Taiwan Inst. Chem. Eng., 91 (2018) 457–467.
[3] M. Bystrzejewski, K. Pyrzyńska, A. Huczko, H. Lange, Carbon-encapsulated magnetic nanoparticles as separable and mobile sorbents of heavy metal ions from aqueous solutions, Carbon, 47 (2009) 1201–1204.
[4] Q. Qiu, X. Jiang, G. Lv, Z. Chen, S. Lu, M. Ni, J. Yan, X. Deng, Adsorption of heavy metal ions using zeolite materials of municipal solid waste incineration fly ash modified by micro wave-assisted hydrothermal treatment, Powder Technol., 335 (2018) 156–163.
[5] Z. Li, L. Wang, J. Meng, X. Liu, J. Xu, F. Wang, P. Brookes, Zeolite-supported nanoscale zero-valent iron: New findings on simultaneous adsorption of Cd(II), Pb(II), and As(III) in aqueous solution and soil, J. Hazard. Mater., 344 (2017) 1–11.
[6] X.M. Zheng, J.F. Dou, M. Xia, A.Z. Ding, Ammonium-pillared montmorillonite-$CoFe_2O_4$ composite caged in calcium alginate beads for the removal of Cs^+ from wastewater, Carbohyd. Polym., 167 (2017) 306–316.
[7] S. Babel, T.A. Kurniawan, Low-cost adsorbents for heavy metals uptake from contaminated water: a review, J. Hazard. Mater., 97 (2003) 219–243.
[8] M. Wang, Y. Zhu, L. Cheng, B. Andserson, X. Zhao, D. Wang, A. Ding, Review on utilization of biochar for metal-contaminated soil and sediment remediation, J. Environ. Sci.-China, 63 (2018) 156–173.
[9] W. Zhang, S. Mao, H. Chen, L. Huang, R. Qiu, Pb(II) and Cr(VI) sorption by biochars pyrolyzed from the municipal wastewater sludge under different heating conditions, Bioresour. Technol., 147 (2013) 545–552.
[10] E.B. Son, K.M. Poo, J.S. Chang, K.J. Chae, Heavy metal removal from aqueous solutions using engineered magnetic biochars derived from waste marine macro-algal biomass, Sci. Total Environ., 615 (2018) 161.
[11] K.B. Cantrell, P.G. Hunt, M. Uchimiya, J.M. Novak, K.S. Ro, Impact of pyrolysis temperature and manure source on physicochemical characteristics of biochar, Bioresour. Technol., 107 (2012) 419–428.
[12] S. Wang, Y. Tang, C. Chen, J. Wu, Z. Huang, Y. Mo, K. Zhang, J. Chen, Regeneration of magnetic biochar derived from eucalyptus leaf residue for lead(II) removal, Bioresour. Technol., 186 (2015) 360–364.

[13] W. Yap, N.M. Mubarak, J.N. Sahu, E.C. Abdullah, Microwave induced synthesis of magnetic biochar from agricultural biomass for removal of lead and cadmium from wastewater, J. Ind. Eng. Chem., 45 (2017) 287–295.
[14] M. Keiluweit, P.S. Nico, M.G. Johnson, M. Kleber, Dynamic molecular structure of plant biomass-derived black carbon (biochar), Environ. Sci. Technol., 44 (2010) 1247–1253.
[15] J.H. Yuan, R.K. Xu, H. Zhang, The forms of alkalis in the biochar produced from crop residues at different temperatures, Bioresour. Technol., 102 (2011) 3488–3497.
[16] J. Zheng, J. Dou, J. Yuan, W. Qin, X. Hong, A. Ding, Removal of Cs^+ from water and soil by ammonium-pillared montmorillonite/Fe_3O_4 composite, J. Environ. Sci.-China, 56 (2017) 12–24.
[17] J. Lu, X. Jiao, D. Chen, W. Li, Solvo thermal synthesis and characterization of Fe_3O_4 and γ-Fe_2O_3 Nanoplates, J. Phys. Chem. C., 113 (2009) 4012–4017.
[18] I. Langmuir, The adsorption of gases on plane surfaces of glass, mica and platinum, J. Chem. Phys., 40 (2015) 1361–1403.
[19] X. Zhou, Y. Liu, J. Zhou, J. Guo, J. Ren, F. Zhou, Efficient removal of lead from aqueous solution by urea-functionalized magnetic biochar: Preparation, characterization and mechanism study, J. Taiwan. Inst. Chem. E., 91 (2018) 457–467.
[20] D. Karamanis, P.A. Assimakopoulos, Efficiency of aluminum-pillared montmorillonite on the removal of cesium and copper from aqueous solutions, Water Res., 41 (2007) 1897–1906.
[21] S. Yang, C. Han, X. Wang, M. Nagatsu, Characteristics of cesium ion sorption from aqueous solution on bentonite- and carbon nanotube-based composites, J. Hazard. Mater., 274 (2014) 46–52.
[22] S. Yang, N. Okada, M. Nagatsu, The highly effective removal of Cs^+ by low turbidity chitosan-grafted magnetic bentonite, J. Hazard. Mater., 301 (2016) 8–16.
[23] A.G. Volkov, S. Paula, D.W. Deamer, Two mechanisms of permeation of small neutral molecules and hydrated ions across phospholipid bilayers, Bioelectrochem. Bioenergetics, 42 (1997) 153–160.
[24] E.R. Nightingale, Phenomenological theory of ion solvation effective radii of hydrated ions, J. Phys. Chem., 63 (1959) 1381–1387.
[25] Z. Yin, Y. Liu, S. Liu, L. Jiang, X. Tan, G. Zeng, M. Li, S. Liu, S. Tian, Y. Fang, Activated magnetic biochar by one-step synthesis: Enhanced adsorption and coadsorption for 17β-estradiol and copper, Sci. Total Environ., 639 (2018) 1530–1542.
[26] C. Souza, D. Majuste, M.S.S. Dantas, V.S.T. Ciminelli, Effect of zinc ion on copper speciation and adsorption on activated carbon, Hydrometallurgy, 176 (2018) 78–86.
[27] K. Li, X. Wang, Adsorptive removal of Pb(II) by activated carbon prepared from Spartina alterniflora: Equilibrium, kinetics and thermodynamics, Bioresour. Technol., 100 (2009) 2810–2815.
[28] C.K. Singh, J.N. Sahu, K.K. Mahalik, C.R. Mohanty, B.R. Mohan, B.C. Meikap, Studies on the removal of Pb(II) from wastewater by activated carbon developed from Tamarind wood activated with sulphuric acid, J. Hazard. Mater., 153 (2008) 221–228.